separations

MDPI

Article

Phase Equilibrium of CO_2 Hydrate with Rubidium Chloride Aqueous Solution

Ryonosuke Kasai, Leo Kamiya and Ryo Ohmura *

Department of Mechanical Engineering, Keio University, 3-14-1 Hiyoshi, Kohoku-ku, Yokohama 223-8522, Japan; r.k.azidesu0214@keio.jp (R.K.); leo25apr@keio.jp (L.K.)
* Correspondence: rohmura@mech.keio.ac.jp; Tel.: +81-455661813

Abstract: Salt lakes are a rich source of metals used in various fields. Rubidium is found in small amounts in salt lakes, but extraction technology on an industrial scale has not been developed completely. Clathrate hydrates are crystalline compounds formed by the encapsulation of guest molecules in cage-like structures made of water molecules. One of the most important properties for engineering practices of hydrate-based technologies is the comprehension of the phase equilibrium conditions. Phase equilibrium conditions of CO_2 hydrate in rubidium chloride aqueous solution with mass fractions of 0.05, 0.10, 0.15 and 0.20 were experimentally investigated in the pressure range from 1.27 MPa to 3.53 MPa, and the temperature was from 268.7 K to 280.6 K. The measured equilibrium temperature in this study decreased roughly in proportion to the concentration of the RbCl solution from the pure water system. This depression is due to the lowering of the chemical potential of water in the liquid phase by the dissolution of RbCl. Experimental results compared with other salt solution + CO_2 hydrate systems showed that the equilibrium temperatures decreased to a similar degree for similar mole fractions.

Keywords: clathrate hydrate; salt lake; CO_2 hydrate; rubidium; phase equilibrium

check for updates

Academic Editors: Xiushen Ye, Dandan Gao and Shiqiang Wang

Received: 20 December 2024
Revised: 8 January 2025
Accepted: 9 January 2025
Published: 11 January 2025

Citation: Kasai, R.; Kamiya, L.; Ohmura, R. Phase Equilibrium of CO_2 Hydrate with Rubidium Chloride Aqueous Solution. *Separations* **2025**, *12*, 13. https://doi.org/10.3390/separations12010013

Copyright: © 2025 by the authors. Licensee MDPI, Basel, Switzerland. This article is an open access article distributed under the terms and conditions of the Creative Commons Attribution (CC BY) license (https://creativecommons.org/licenses/by/4.0/).

1. Introduction

1.1. Extraction of Metals from Salt Lakes

Alkali and alkaline earth metals such as lithium, potassium, and magnesium are abundant in salt lake brine [1,2]. These metals are extracted from brine and are widely used in various fields. Solar evaporation precipitation is a widely used technology to obtain metals from brine [3,4], but there are problems such as low recovery rates, high costs, and ecological impacts [4,5]. Plenty of novel extraction technologies for metals (especially lithium) adsorption, membrane, etc., have been proposed to efficiently obtain them [4]. In the adsorption method, adsorbents such as ion-sieve oxides enable the extraction of only specific metal ions from multiple types of ions in brine [4,6]. Membrane technology used in various industries is environmentally friendly and less energy-consuming. This technology is classified into three categories according to the driving force of the process: nanofiltration (pressure-driven), liquid membrane (chemical potential-driven), and electrodialysis and membrane electrolysis (electrical potential-driven) [4,7,8].

There are metals in very small amounts in salt lake brine, one of which is rubidium. Rubidium is a rare alkali metal used in electronic devices, specialty glasses, alkali vapor lasers, atomic clocks, etc. [9–11]. However, although the total content of rubidium in salt lake brine is enormous, there is no technology to extract it from brine industrially. Currently, rubidium is extracted from mineral resources using either acid digestion or

roasting–leaching methods [9]. The acid digestion method uses the properties of lepidolite and pollucite, containing rubidium, to be easily eroded by acids such as sulfuric acid [12,13]. The roasting–leaching method involves adding sodium or calcium salts to the lepidolite and pollucite and roasting it at high temperatures to destroy the mineral phase and obtain rubidium by water leaching [14,15]. Rubidium is also contained in seawater, but the salt lake brine contains much more. Technologies for extracting rubidium from salt lake brine are required for the comprehensive use of the resources contained in it.

1.2. Clathrate Hydrate

Clathrate hydrates (hereafter hydrates) are ice-like crystalline compounds composed of water and guest molecules under low temperature and high-pressure conditions [16]. The guest molecules are encapsulated in cage-like structures formed by hydrogen-bonded water molecules (host molecules). There are five different cage structures composed of water molecules: 5^{12} (dodecahedron consisting of 12 pentagons), $5^{12}6^2$ (tetradecahedron composed of 12 pentagons and 2 hexagons), $5^{12}6^4$ (hexadecahedron consisting of 12 pentagons and 4 hexagons), $5^{12}6^8$ (icosahedron composed of 12 pentagons and 8 hexagons) and $4^35^66^3$ (dodecahedron consisting of three squares, six pentagons, and three hexagons). Hydrate has three canonical types of crystal structure: structure I (sI), structure II (sII), and structure H (sH). Structure I hydrate is composed of 5^{12} and $5^{12}6^2$ cages, structure II (sII) is 5^{12} and $5^{12}6^4$ cages, and structure H (sH) is 5^{12} and $5^{12}6^8$, and $4^35^66^3$. The guest compounds determine the name of the hydrate: if CO_2 is captured in the cage, it is called CO_2 hydrate. Hydrate was first recognized in the 1930s as a cause of blockages in natural gas pipelines. Hydrate has been studied to identify various characteristics such as large gas storage density [16], and guest compound selectivity [17].

Hydrate-based technology related to salt lakes and salt water, such as lithium enrichment [18], seawater desalination [19,20], and natural gas storage [21,22] are attracting attention. These technologies are based on the characteristic that the electrolytes are not encapsulated in the hydrate cages [23]. In hydrate-based lithium enrichment, hydrates are formed in lithium-aqueous solutions such as salt lake brine. Lithium ions are concentrated in the liquid phase because water forms hydrate with guest compounds, and lithium ions are not contained in the hydrate. Lithium is usually obtained by evaporating salt lake brine, but the hydrate-based method does not require higher temperatures and takes less time than the evaporation method.

Hydrate-based seawater desalination technology is implemented by forming hydrate with seawater. Since the components of hydrate are only water and guest compounds, fresh water can be obtained by decomposing the hydrate with thermal stimulation or depressurization. The reverse osmosis membrane (RO) method, the most widely used desalination technology, has drawbacks. The operational seawater concentration needs to be less than approximately 7%, the water recovery ratio is less than 55%, and the highly concentrated seawater is discharged to the ocean. Hydrate-based desalination has no operational concentration limitations. It is reported that this technology would surpass RO methods in terms of water recovery ratio and energy consumption [20]. Furthermore, this technology is expected to produce salt simultaneously because the salts in the liquid phase (seawater) would be concentrated at the eutectic point in this process [24]. Because of the abovementioned advantages, hydrate-based desalination is expected to be a zero-liquid discharge (ZLD) process.

Storing and transporting natural gas in the form of hydrates has attracted much attention. It has been proposed that hydrates containing natural gas from seawater, which is abundant in nature, be produced. This technology is advantageous because natural gas hydrates are non-explosive, environmentally friendly, and can store natural gas in small

volumes. Compared to conventional natural gas storage methods, this technology can store natural gas at higher temperatures than liquefied natural gas (LNG) and lower pressures than compressed natural gas (CNG).

1.3. Phase Equilibrium Conditions

For the engineering practice of these hydrate-based technologies, it is necessary to understand the difference in kinetics of hydrate between pure water and saltwater systems. One of the most crucial differences is the phase equilibrium conditions. Phase equilibrium conditions are the temperature and pressure where the chemical potentials of all phases are equal. A *p*-*T* diagram is frequently used to show the phase equilibrium conditions in hydrate present systems. The Gibbs phase rule shown in Equation (1) is satisfied in an equilibrium state.

$$f = c - p + 2 \quad (1)$$

f, c, and p represent the degree of freedom, the number of components, and phases. At three-phase equilibrium (liquid water (L_w) + vapor guest compounds (V) + hydrate (H)), the degree of freedom in this system is unity because the values of c and p are two and three. At L_w + V + H three-phase equilibrium, since determining the temperature automatically determines the pressure, the phase equilibrium conditions illustrate a line, as shown in Figure 1. This *p*-*T* diagram indicates the three-phase equilibrium conditions of CO_2 hydrate in the pure water system [25]. CO_2 hydrates are formed at lower temperatures and higher pressures than this line. At the three-phase equilibrium in this study (RbCl aqueous solution + CO_2 + hydrate), the number of components and phases of this system are four and three because of the addition of rubidium chloride. According to the Gibbs phase rule, this system has two degrees of freedom. However, since the concentration of the aqueous solution is specified, the degree of freedom remains unity as in the pure water system above.

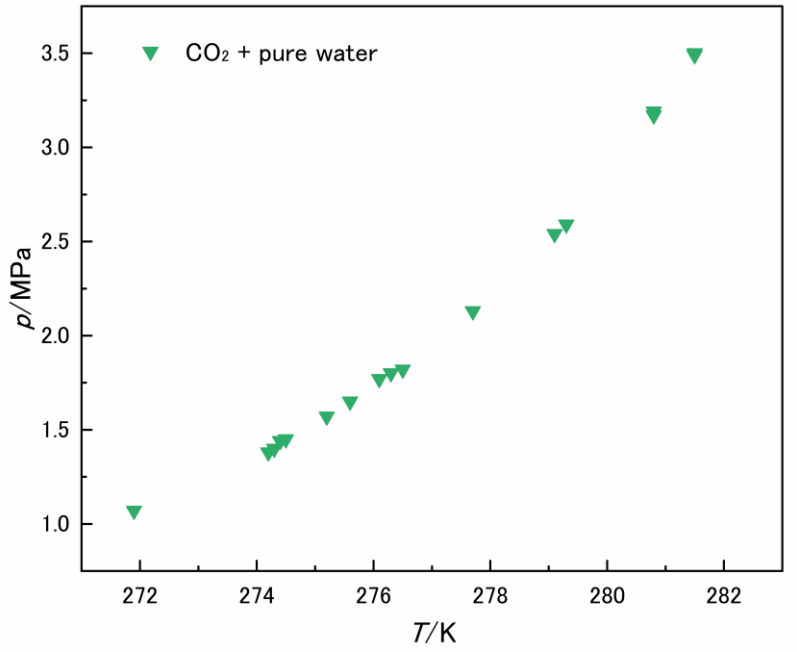


Figure 1. Phase equilibrium conditions of CO_2 hydrate in pure water system [25].

The phase equilibrium conditions are required for the comprehension of the mechanical properties of hydrate solids. The phase equilibrium condition is essential for initiating engineering thermodynamic treatments. The driving force of kinetics is derived from the disparities between equilibrium conditions and experimental conditions, such

as subcooling temperature, excessive pressure, or variations in chemical potential. Thus, the phase equilibrium conditions serve as the foundational basis for comprehension of kinetics. Comprehension of the three-phase equilibrium conditions is also essential for the engineering practice of hydrate-based technologies because understanding equilibrium conditions facilitates the operation of hydrate formation and decomposition. Moreover, this understanding is also advantageous for manipulating the crystal morphology of hydrates, thereby improving the efficiency of the overall process. The primary challenge in the separation of RbCl from salt lake brine is the effective separation from other coexisting electrolytes, which are present at high concentrations and have chemical properties similar to RbCl. The phase equilibrium data provide the fundamental basis for understanding and addressing this separation process. In previous studies, equilibrium conditions of hydrate in salt-containing aqueous solutions such as sodium chloride, potassium chloride, and calcium chloride solution have been experimentally measured at various concentrations [26–28].

1.4. Prediction of Equilibrium by Thermodynamic Statistical Model

In addition to these experimental measurements, thermodynamic statistical models have been used to predict the phase equilibrium conditions of various aqueous solutions as described below. Van der Waals and Platteeuw (1959) reported a method for calculating the chemical potential of water in the hydrate phase [29], which enabled phase equilibrium calculations in systems containing hydrates. The Pitzer model was used to calculate the chemical potential of the liquid phase [30]. A Pitzer model that accounts for high-concentration electrolyte solutions is incorporated into the vdW-P model to reproduce the phase equilibrium conditions of hydrates in the electrolyte aqueous system. The phase equilibrium calculation program is based on the model developed by Van der Waals and Platteeuw model (referred to as the vdW-P model). The three-phase equilibrium conditions are established by assuming a pressure at a certain temperature and calculating the chemical potential of the hydrate phase and the aqueous phase using Equations (2)–(4) iteratively changing the pressure for calculations. The three-phase equilibrium conditions are the temperature and pressure conditions at which Equation (2) holds.

In the vdW-P model, the chemical potential of water in the hydrate phase is expressed as in Equation (2) by establishing the following assumptions (i) to (iv).

(i) There is no interaction between the guest and host molecules
(ii) Each cage can hold a maximum of one guest molecule.
(iii) There are no interactions between guest molecules.
(iv) Quantum effects can be neglected, and the system can be described using classical statistical thermodynamics.

$$\Delta\mu_W^H = \Delta\mu_W^L \tag{2}$$

$$\Delta\mu_W^L = \mu_W^\beta - \mu_W^L \tag{3}$$

$$\Delta\mu_W^H = -RT\sum_{\mathrm{i}} \nu_i \ln\left(1 - \sum_k \theta_{ki}\right) \tag{4}$$

In Equation (2), μ is the chemical potential, H refers to the hydrate phase, W refers to water, R is the ideal gas constant, T is the absolute temperature, ν_i is the number of type-i (i = small or large in sI and sII) cages per water molecule, and θ_{ki} is the occupancy of type-i cages by k-type molecules. To solve this equation for the chemical potential, it is necessary to determine the Langmuir constant C_{ki} and the cage occupancy θ_{ki}. The Langmuir constant C_{ki} is shown in Equation (5), and the cage occupancy θ_{ki} is shown in Equation (6).

$$C_{\mathrm{ki}} = \frac{4\pi}{k_{\mathrm{B}}T} \int_0^{R_{\mathrm{fc}}-a} \exp\left(-\frac{w(r)}{k_{\mathrm{B}}T}\right) r^2 dr \tag{5}$$

$$\theta_{ki} = \frac{C_{ki} f_k}{1 + \sum_k C_{ki} f_k} \tag{6}$$

In Equation (5), k_B is the Boltzmann constant, and R_{fc} is the distance to the guest molecules from the center of the most fugacious cage. Fugacity is a corrected pressure that accounts for the difference in free energy between real and ideal gases. In Equation (6), C_{ki} is the Langmuir constant, and f_k is the fugacity. The Kihara potential $w(r)$ is represented as follows.

$$w(r) = 2z\varepsilon\left[\frac{\sigma^{12}}{R_{\mathrm{fc}}^{11} r}\left(\delta^{10} + \frac{a}{R_{\mathrm{fc}}}\delta^{11}\right) - \frac{\sigma^{6}}{R_{\mathrm{fc}}^{5} r}\left(\delta^{4} + \frac{a}{R_{\mathrm{fc}}}\delta^{5}\right)\right] \tag{7}$$

a, σ, and ε refer to the parameters of the intermolecular interaction potential—also known as the Kihara parameters—which indicate the sphere radius, the distance at which the potential is zero (the balance between attractive and repulsive forces), and the maximum value of the potential. The chemical potential of water in the hydrate phase can be derived by calculating the cage occupancy θ_{ki}. The vdW-P model is the foundation for the phase equilibrium calculation program in systems containing hydrates. Numerical methods to represent and predict the hydrate phase equilibrium are summarized in the recent review article by Yasuda and Ohmura [31].

In an electrolyte aqueous system, the chemical potential of the water changes with a mass fraction of the electrolyte. To calculate the activity coefficient of water, the formula developed by Englezos and Bishnoi [30], based on the model of Pitzer, was used. This model calculates the activity coefficient of water as being influenced only by the presence of electrolytes. This formula is derived by integrating the Gibbs–Duhem equation with a single electrolyte solution.

$$\Delta\mu_W^L = \mu^\circ + RT\ln(a_w x) \tag{8}$$

$$I = \frac{1}{2}\sum_i m_i z_i^2 \tag{9}$$

$$\ln a_w = \frac{-18vm}{1000}\left(1 + |\mathrm{z}_-\mathrm{z}_+|\theta_1 + m\theta_2 + m^2\beta_2\right) \tag{10}$$

$$\theta_1 = \mathrm{A}_\Phi\left\{\frac{I^{\frac{1}{2}}}{1 + 1.2^{\frac{1}{2}}}\right\} \tag{11}$$

$$\theta_2 = \beta_0 + \left\{\beta_1 \exp\left(-2I^{\frac{1}{2}}\right)\right\} \tag{12}$$

Here, the A_Φ is subscripted Debye−Hückel coefficient. m represents the molar concentration, v is the number of moles of ions per mole of salt, z is the charge number, I is the ionic strength, and β_0, β_1, and β_2 are constants that differ according to the type of salt. As shown in Equation (10), the activity coefficient of water, which determines the chemical potential of water in the liquid phase, depends on only the molar concentration of the aqueous solution. In an electrolyte aqueous system, while the chemical potential of water in the solid (ice) phase remains unchanged, the chemical potential in the liquid phase decreases. The difference in chemical potential between the solid and liquid phases causes a freezing point depression. Because the same phenomenon occurs in the electrolytes aqueous solution and hydrate system, the phase equilibrium temperature of the hydrate also decreases.

1.5. Measurements of Phase Equilibrium

There are three methods for experimental measurements of three-phase equilibrium conditions: isothermal, isobaric, and isochoric [32]. The isothermal method measures phase equilibrium conditions by injecting and releasing guest compounds under constant temperature conditions. However, large amounts of gas are used for experiments with this method. The isobaric method measures phase equilibrium conditions by varying temperature under constant pressure. Because visual observations recognize the presence of hydrate in this method, the results become unstable. In the isochoric method, phase equilibrium conditions are measured by cooling and heating system temperature with constant volume conditions. Although the cooling rate does not affect the measurement results, the heating rate significantly affects them. Continuous and stepwise heating are two ways to increase the temperature using the isochoric method. It is reported that stepwise heating can obtain accurate values because the system temperature is raised after the pressure reaches a steady state [32]. Because of the descriptions above, the isochoric method with stepwise heating was employed in this study to obtain phase equilibrium conditions.

As described above, previous studies have experimentally measured three-phase equilibrium conditions in salt systems. It is reported that the phase equilibrium temperatures of hydrate in an electrolyte aqueous solution are lower than in a pure water system. However, the measurements of the equilibrium conditions of CO_2 hydrate in rubidium chloride aqueous solution have not been conducted yet. The concentration of RbCl in natural salt lakes is typically very low, and its impact on hydrate phase equilibrium conditions is minimal. Although the mass fractions of RbCl chosen for our experiments were significantly higher than the natural salt lakes, this study would generalize the effects of electrolytes from the perspective of mass fraction and mole fraction and provide broader insights into the behavior of RbCl under hydrate-forming conditions. Experimental results for this system would facilitate understanding the effects of salts like rubidium on hydrates and improve the accuracy of prediction for the equilibrium conditions by statistical thermodynamic models. CO_2 was employed because it is the most utilized industrial gas, and the phase equilibrium of CO_2 hydrate (274.3 K, 1.40 MPa) [25] is more moderate than that of common gases such as methane (273.6 K, 2.673 MPa) [33], N_2 (274.55 K, 19.09 MPa) [34], and O_2 (273.8 K, 13.56 MPa) [34]. Moreover, the formation of hydrates with carbon dioxide can be effectively utilized for carbon capture, utilization, and storage (CCUS), as the phase equilibrium conditions are comparatively favorable. In this study, we measured the three-phase equilibrium conditions of CO_2 hydrate in RbCl aqueous solution with mass fractions of 0.05, 0.10, 0.15, and 0.20.

2. Materials and Methods

The compounds employed in this study were rubidium chloride with a mass-based purity of 99.0% (Tokyo Chemical Industry Co., Ltd., Tokyo, Japan) and carbon dioxide with a mole-based purity of 99.99% (Dalian Taiyo Nippon Sanso Gas Co., Ltd., Tokyo, Japan).

The schematic diagram of the experimental apparatus is shown in Figures 2 and 3. Because the phase equilibrium conditions are specified by the pressure and temperature, state functions, in the isochoric method, there is no difference in the phase equilibrium conditions obtained using different apparatuses, and data consistency is guaranteed. The pressure-resistant vessels (1) and (2) are made of stainless steel. The inner dimension diameter of vessel (1) is 80 mm, the depth is 40 mm, and the inner volume is 200 cm^3. The inner dimension diameter of vessel (2) is 20 mm, the depth is 92 mm, and the inner volume is 65 cm^3. These vessels were immersed in ethylene glycol solution baths. The temperatures of the baths were controlled by PID controlled heater (model TR-2α, As One Co., Ltd., model BF400, Yamato Scientific Co., Ltd., Tokyo, Japan) and an immersion cooler (ECS-30,

Tokyo Rikakikai Co., Ltd., Tokyo, Japan, model BE201, Yamato Scientific Co., Ltd., Tokyo, Japan). The temperatures inside the cells were varied by changing the temperature of the ethylene glycol solution. The temperature of the ethylene glycol solution was measured by two platinum resistance thermometers (Reference Calibration Thermometer, Electronic Temperature Instruments Ltd., Worthing, U.K., expanded uncertainty was ±0.1 K). These thermometers were used to measure the temperature of ethylene glycol at two different points in the ethylene glycol bath. After confirming the difference between their values to be less than the expanded uncertainty, the average of the two was recorded. The pressure in the cell was measured by a strain-gauge pressure transducer (model PG-50KU and model PG-100KU, Kyowa Electronic Instruments Co., Ltd., Tokyo, Japan) and tracked by the data logger (model GL840, Graphtec Co., Ltd.). The formation and decomposition of hydrate were accelerated by stirring the vessel with an electromagnetic stirrer (Nitto Koatsu Co., Tokyo, Japan).

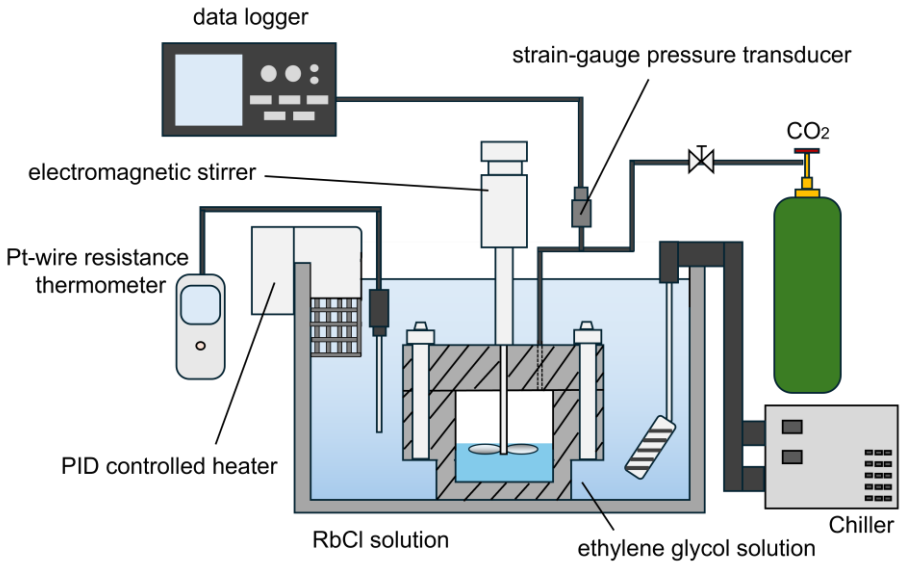


Figure 2. Schematic diagram of experimental apparatus (1).

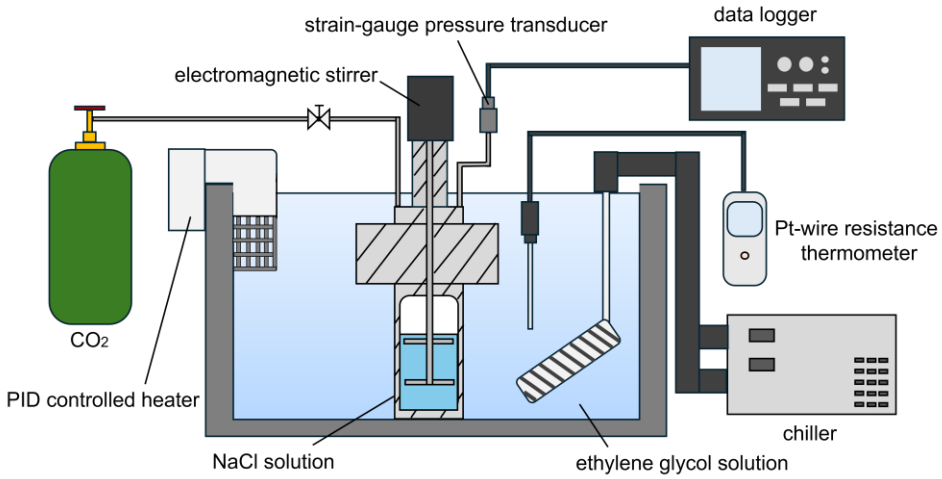


Figure 3. Schematic diagram of experimental apparatus (2).

The isochoric method was employed as described in the introduction for three-phase equilibrium conditions measurements. This method is most frequently used for measuring phase equilibrium conditions, using hydrate formation and decomposition [35–38]. Figure 4 shows the *p*-*T* history obtained with the isochoric method in this study. The detailed procedure is as follows. Supply water (rubidium chloride aqueous solution in this study)

to the vessel. After depressurizing the cell to less than 0.01 MPa, the guest compound (CO_2 in this study) is supplied to a given pressure. The temperature is set where hydrate will not form. It is noted that the temperature and pressure at a steady state are recorded as the initial conditions. The vessel was then cooled to form hydrate. Hydrate formation may be observed by a sudden drop in pressure, as shown in Figure 4. After confirming the pressure drop, the temperature is increased to decompose the hydrate. If hydrate decomposes, the pressure in the vessel increases significantly because the gas encapsulated in the hydrate is released. After the pressure rise stops, the temperature is raised again. Repeat this operation until all hydrate is decomposed. In this study, the data were measured at the step of 0.1 K. When there is no hydrate in the cell, the pressure increases slightly with increasing temperature. Since the increase in pressure varies depending on the presence or absence of hydrate, the slope of the *p*-*T* diagram changes at a certain point. Because all hydrates may be decomposed at this point, the condition just before this point where hydrate certainly exists is defined as the three-phase equilibrium condition. In Figure 4, the initial condition was 271.7 K and 1.31 MPa. The vessel was cooled from this condition, and hydrate formation occurred. The system became a steady state at 267.8 K and 1.15 MPa. The temperature was increased at the step of 0.1 K, and steady-state conditions were recorded. The slope of these plots changed after 268.8 K. 268.7 K and 1.27 MPa; the condition just before this point is a three-phase equilibrium condition obtained from this measurement.

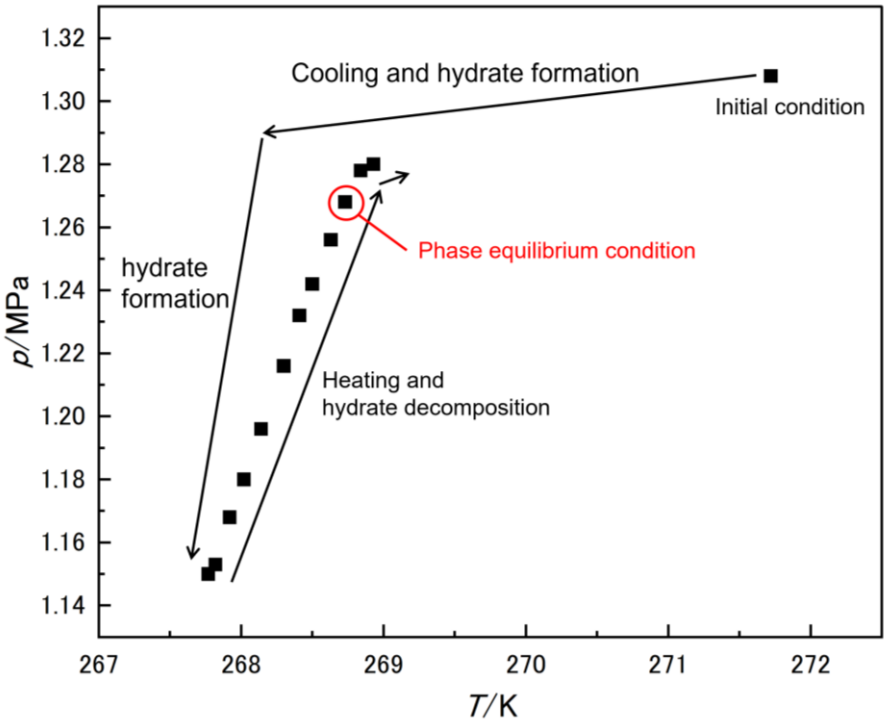


Figure 4. *p*-*T* history of isochoric method in this study.

Rubidium chloride aqueous solutions with mass fractions of 0.05, 0.10, 0.15, and 0.20 were made by mixing distilled water and solid reagent rubidium chloride indicated in Table 1. Three-phase equilibrium conditions were measured at the four concentrations using the isochoric method from various initial conditions.

Table 1. The amount of water and RbCl for a given concentration.

Mass Fraction	Water [g]	RbCl [g]
0.05	28.5	1.5
0.10	36.0	4.0
0.15	34.0	6.0
0.20	40.0	10.0

3. Results and Discussion

3.1. Phase Equilibrium of CO_2 Hydrate with Rubidium Chloride Aqueous Solution

The measured L + V + H three-phase equilibrium conditions of CO_2 hydrate in rubidium chloride aqueous solution are shown in Table 2. The reliability and repeatability of measurements using the same apparatus were demonstrated in the previous studies [25,39,40]. Figure 5 shows the *p*-*T* diagram of phase equilibrium data obtained in the present and previous studies [25]. The expanded uncertainty of temperature was ±0.1 K, and the uncertainty of pressure was ±0.03 MPa. The inverted triangle represents the phase equilibrium conditions of CO_2 hydrate in the pure water + CO_2 system. The squares, circles, triangles, and diamonds represent the phase equilibrium conditions in the rubidium chloride aqueous solution + CO_2 systems with mass fractions of 0.05, because the phase equilibriums are 0.10, 0.15, and 0.20 obtained in this study. The curves drawn for the four aqueous solutions are approximations using the Clausius–Clapeyron Equation (13) described below. As shown in Figure 5, the phase equilibrium conditions shifted toward the lower temperature and higher pressure with the increased concentration of rubidium chloride aqueous solution. Hydrate formation was inhibited by electrolytes, as reported in the previous studies. As described in the introduction, the activity coefficient, which determines the chemical potential of water, depends on the presence of electrolytes. Because the chemical potential of water in the liquid phase decreases with increasing the mole fraction of RbCl, the phase equilibrium conditions where the chemical potentials of the three phases are equal moved to lower temperature and higher pressures at more elevated concentrations. To assess the internal consistency of the data newly obtained in the present study, the Clausius–Clapeyron Equation (13) was employed.

$$\ln(p/\mathrm{MPa}) = a(T/\mathrm{K})^{-1} + b \tag{13}$$

The fitting parameters *a* and *b* are dimensionless. This equation represents the temperature and pressure at phase equilibrium conditions linearly on the $\ln p - 1/T$ diagram. Figure 6 shows the $\ln p - 1/T$ diagram of phase equilibrium conditions data measured in this study. As shown in the $\ln p - 1/T$ diagram, the plots were aligned approximately in a straight line at a given concentration. Table 3 shows the values of a, b, and the coefficient of determination R^2 of the straight lines approximated with Equation (13) from the data experimentally measured at mass fractions of 0.05, 0.10, 0.15, and 0.20. Figure 7 shows the deviation between the phase equilibrium temperature obtained in this study and calculated from the Clausius–Clapeyron equation using the fitting parameter in Table 3 for a given concentration. The vertical and horizontal axes represent the difference in equilibrium temperatures and pressure. The average absolute deviations of the measured values from the calculated one at mass fractions with 0.05, 0.10, 0.15, and 0.20 were 0.0819 K, 0.0403 K, 0.0437 K and 0.0174 K, less than the expanded uncertainty of measurements. From the above discussion, the experimentally obtained data are consistent with the Clausius–Clapeyron equation. The data shown in Figure 7 also confirm the consistency of the data obtained with two different apparatuses. For comparing the phase equilibrium temperatures of each concentration at given pressures, the plots on the *p*-*T* diagram were interpolated and

extrapolated by exponential functions. Table 4 shows the phase equilibrium temperatures obtained by this interpolation and extrapolation for pure water and the rubidium chloride aqueous solutions systems at 1.5, 2.0, 2.5, 3.0, and 3.5 MPa. It should be noted that the consistency with the Clausius–Clapeyron equation in pure water and CO_2 systems is clearly described in the previous study [25]. Figure 8 shows the degree of decrease in the phase equilibrium temperatures of an aqueous solution system from a pure water system at a given pressure. The horizontal and vertical axes represent the mass fraction of solutions and the degree of depression in phase equilibrium temperature. As shown in Figure 8, the degree of decrease in the phase equilibrium temperature is roughly proportional to the mass fraction of the solutions. On the other hand, this degree does not change with increasing pressure.

Table 2. Three-phase equilibrium conditions of CO_2 hydrate with RbCl solutions.

Mass Fraction	*T* [K]	*P* [MPa]
0.05	275.5	1.84
0.05	273.1	1.40
0.05	280.6	3.56
0.05	278.6	2.72
0.10	276.7	2.47
0.10	275.1	2.01
0.10	273.1	1.58
0.10	279.3	3.53
0.10	278.0	2.96
0.15	273.1	1.80
0.15	270.7	1.37
0.15	277.7	3.34
0.15	276.6	2.80
0.15	274.8	2.23
0.20	274.3	2.58
0.20	271.5	1.82
0.20	268.7	1.27
0.20	276.5	3.41

Table 3. The fitting parameter for Equation (13) and coefficient of determination R^2.

Mass Fraction	a	b	R^2
0.05	−9637	35.6	0.9981
0.10	−9956	36.9	0.9977
0.15	−9536	35.5	0.9967
0.20	−9468	35.5	0.9999

Table 4. Phase equilibrium temperatures of CO_2 hydrate calculated from interpolation and extrapolation of measured data by the Clausius–Clapeyron equation.

	Equilibrium Temperature [K]				
Mass Fraction	**1.5 MPa**	**2.0 MPa**	**2.5 MPa**	**3.0 MPa**	**3.5 MPa**
0	274.80	277.11	278.91	280.37	281.61
0.05	273.79	276.08	277.85	279.30	280.53
0.10	272.79	274.99	276.7	278.09	279.28
0.15	271.55	273.82	275.57	277.01	278.23
0.20	270.02	272.27	274.02	275.45	276.67

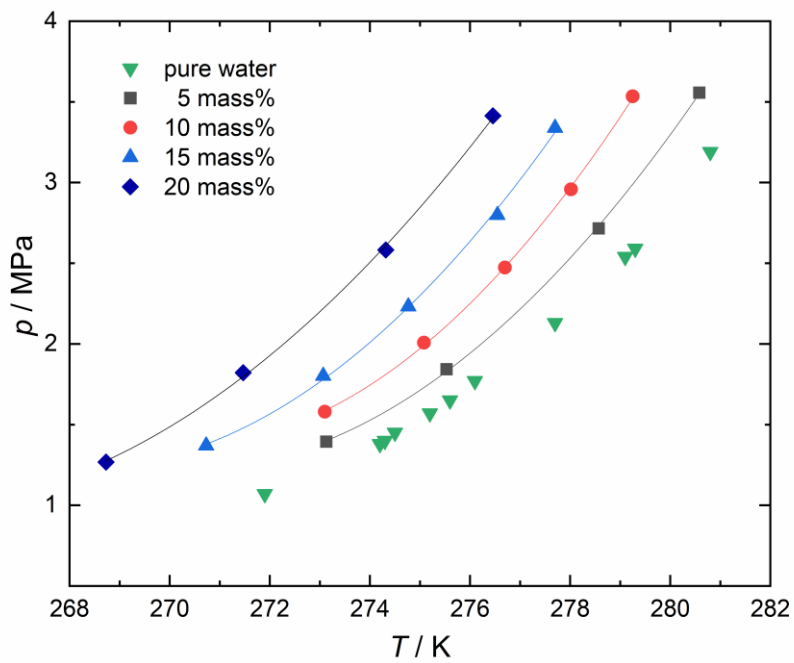


Figure 5. *p-T* diagram of phase equilibrium conditions of CO_2 hydrate in pure water and RbCl solution. Inverted triangle: pure water [25]; Square: 5 mass% RbCl solution (this study); Circle: 10 mass% RbCl solution (this study); Triangle: 15 mass% RbCl solution (this study); Diamond: 20 mass% RbCl solution (this study).

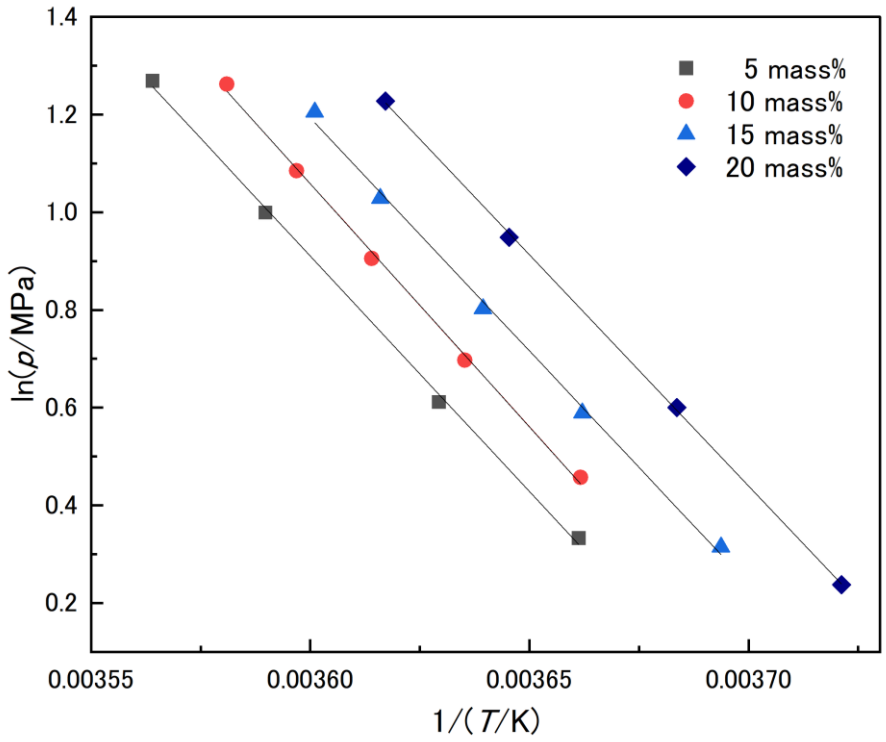


Figure 6. $\ln p - 1/T$ diagram of phase equilibrium conditions of CO_2 hydrate in RbCl aqueous solution.

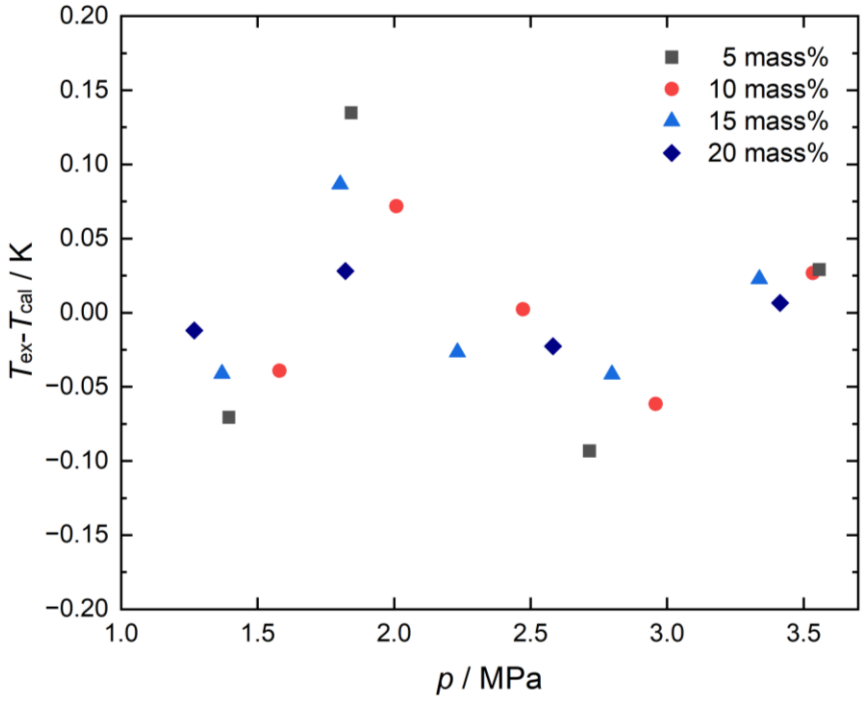


Figure 7. The deviation between the CO_2 hydrate equilibrium temperature of obtained from experiments and calculated from the Clausius–Clapeyron equation.

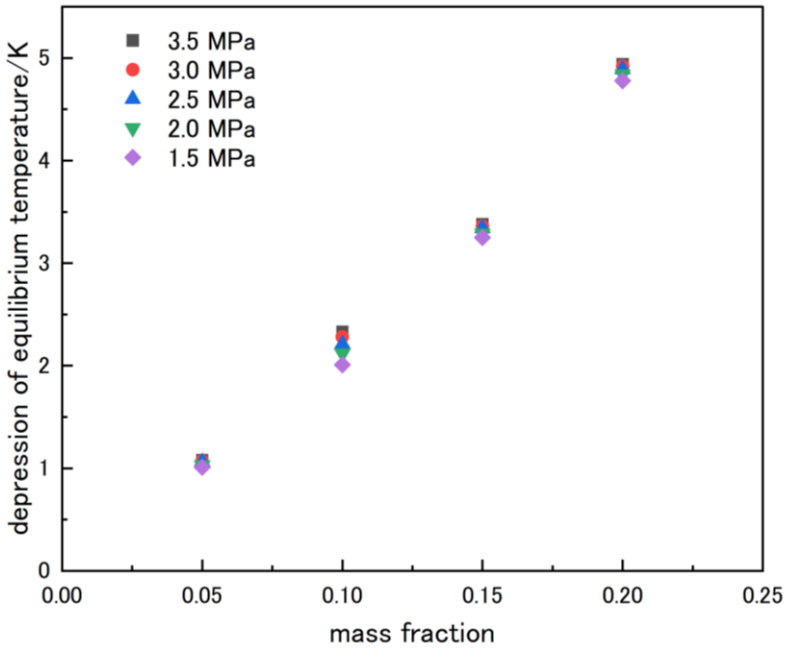


Figure 8. The degree of decrease in the phase equilibrium temperatures of the RbCl solution system from the pure water system.

3.2. Comparison with Other Electrolytes Aqueous Solution

Three-phase equilibrium conditions of CO_2 hydrate in RbCl, NaCl and $CaCl_2$ aqueous solution measured in the present and previous studies [25–28] are shown in Figure 9. RbCl solution with mass fractions of 0.10 and 0.20 are the results of this study, while the data of NaCl with mass fractions of 0.05 and 0.10 and $CaCl_2$ with mass fraction of 0.10 are from the previous studies. The mole fractions at given mass fractions are in Table 5. Their mole fractions were calculated using the molar masses of RbCl, NaCl and $CaCl_2$ as 120.9 kg/kmol, 58.4 kg/kmol and 111.0 kg/kmol. As shown in Table 5, the mole fractions of rubidium

chloride and sodium chloride aqueous solutions with mass fractions of 0.10, 0.20, and 0.05, 0.10 are approximately the same. Since both RbCl and NaCl are assumed to be entirely ionized, the mole fractions of electrolytes are also almost the same. The degree of decrease in the phase equilibrium temperatures of NaCl and RbCl at 3.0 MPa with mass fractions of 0.05 and 0.10 was 1.96 K and 2.29 K. With the mass fractions of 0.10 and 0.20, the degrees of decrease were 4.77 K and 4.93 K at 3.0 MPa. Comparing RbCl and $CaCl_2$ solutions with mass fraction of 0.10, the mole fraction of the $CaCl_2$ solution is approximately 1.09 times that of the RbCl solution. However, the degree of depression in the phase equilibrium temperature of the $CaCl_2$ solution at 3MPa was 4.24 K, which is 1.85 times that of the RbCl solution. The activity coefficient of water, which determines the chemical potential of water in the liquid phase, is influenced only by the presence of electrolytes. The magnitude of the effect is ion-specific and depends on the molar concentration of electrolytes and ion–water interactions. Comparing the RbCl and NaCl solutions with similar mole fractions, the depression of phase equilibrium temperature is almost the same because the differences in chemical potentials of the water in the liquid phase are similar. The slightly larger decrease in phase equilibrium temperature of the rubidium chloride aqueous solution is ascribed to the larger mole fraction of the aqueous solution and ion–water interactions. Because RbCl and $CaCl_2$ ionize to two and three ions, the degree of depression in the $CaCl_2$ solution system is significantly larger even in similar mole fractions. Table 5 and Figure 9 indicate the correlation of the concentrations and equilibrium temperature differences. As mentioned in the introduction, there is an approach to using a statistical thermodynamic model to predict the phase equilibrium conditions of hydrates in salt systems. These results would contribute to improving the accuracy of that prediction.

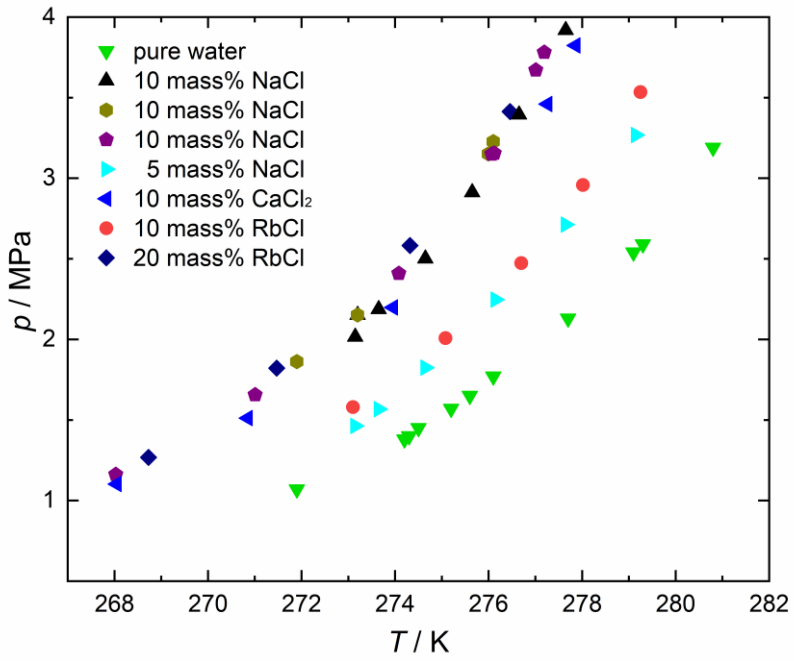


Figure 9. The comparison of RbCl, NaCl and $CaCl_2$ solution in CO_2 hydrate systems. Inverted triangle: pure water [25]; Triangle: 10 mass% NaCl solution [26]; Hexagonal: 10 mass% NaCl solution [27]; Pentagonal: 10 mass% NaCl solution [28]; Right-pointing triangle: 5 mass% NaCl solution [26]; Left-pointing triangle: 10 mass% $CaCl_2$ solution [28]; Circle: 10 mass% RbCl solution (this study); Diamond: 20 mass% RbCl solution (this study).

Table 5. The mole fraction of the RbCl, NaCl and $CaCl_2$ solutions corresponding to the mass fraction.

Mass Fraction	Mole Fraction
10 mass% RbCl	0.0163
20 mass% RbCl	0.0359
5 mass% NaCl	0.0160
10 mass% NaCl	0.0331
10 mass% $CaCl_2$	0.0177

4. Conclusions

Three-phase equilibrium conditions of CO_2 hydrate in rubidium chloride aqueous solution were experimentally measured at the mass fractions of 0.05, 0.10, 0.15, and 0.20. The phase equilibrium conditions shifted toward lower temperature and higher pressure as the mass fraction of rubidium chloride increased. The three-phase equilibrium temperatures of rubidium chloride aqueous solutions with mass fractions of 0.05, 0.10, 0.15, and 0.20 decrease by 1.1 K, 2.2 K, 3.3 K and 4.9 K from that of a pure water system. These results indicate that rubidium chloride inhibited the hydrate formation. This depression in phase equilibrium temperature occurs because the chemical potential of water, reduced by electrolyte dissolution, is equal to the chemical potential of the hydrate phase at lower temperatures. Phase equilibrium conditions of CO_2 hydrates in sodium chloride and rubidium chloride aqueous solutions with almost the same mole fractions were compared. It was experimentally shown that the degree of decrease in phase equilibrium temperature from the pure water + CO_2 system depends on the aqueous solution's mole fraction. The equilibrium temperature of sodium chloride and rubidium chloride aqueous solutions with mole fractions of 0.0160 and 0.0163 decreased by 1.96 K and 2.29 K. With the mole fractions of 0.0331 and 0.0359, the degrees of decrease were 4.77 K and 4.93 K. Because the mole fractions of rubidium chloride solution were larger than those of sodium chloride and there is ion–water interaction, the decreases of equilibrium temperature of rubidium chloride solution were slightly larger. The degree of depression in phase equilibrium temperature in the $CaCl_2$ solution system was 1.85 times that in the RbCl solution system at a similar mole fraction. These results would facilitate understanding the effects of rubidium chloride and electrolytes on hydrate formation and improve the accuracy of predicting phase equilibrium conditions for hydrates in salt systems.

Author Contributions: Conceptualization, R.K., L.K. and R.O.; methodology, R.K. and L.K.; validation, formal analysis, L.K.; investigation, R.K. and L.K.; data curation, R.K. and L.K.; writing—original draft preparation, R.K. and L.K.; writing—review and editing, L.K. and R.O.; visualization, L.K.; supervision, R.O.; project administration, R.O. All authors have read and agreed to the published version of the manuscript.

Funding: This research was funded by the Keirin-racing-based research-promotion fund from the JKA Foundation, grant number 2024M-550.

Data Availability Statement: The data presented in this study are available upon request from the corresponding author.

Acknowledgments: The authors are grateful for the System Brain Inc. (Gunma, Japan) for arranging reagents.

Conflicts of Interest: The authors declare no conflicts of interest.

References

1. Liu, S.-M.; Liu, H.-H.; Huang, Y.-J.; Yang, W.-J. Solvent extraction of rubidium and cesium from salt lake brine with t-BAMBP–kerosene solution. *Trans. Nonferrous Met. Soc. China* **2015**, *25*, 329–334. [CrossRef]

2. Naidu, G.; Jeong, S.; Johir, A.H.; Fane, A.G.; Kandasamy, J.; Vigneswaran, S. Rubidium extraction from seawater brine by an integrated membrane distillation-selective sorption system. *Water Res.* **2017**, *123*, 321–331. [CrossRef] [PubMed]
3. Pranolo, Y.; Zhu, Z.; Cheng, C.Y. Separation of lithium from sodium in chloride solutions using SSX systems with LIX 54 and Cyanex 923. *Hydrometallurgy* **2015**, *154*, 33–39. [CrossRef]
4. Liu, G.; Zhao, Z.; Ghahreman, A. Novel approaches for lithium extraction from salt-lake brines: A review. *Hydrometallurgy* **2019**, *187*, 81–100. [CrossRef]
5. Tadesse, B.; Makuei, F.; Albijanic, B.; Dyer, L. The beneficiation of lithium minerals from hard rock ores: A review. *Miner. Eng.* **2019**, *131*, 170–184. [CrossRef]
6. Swain, B. Recovery and recycling of lithium: A review. *Sep. Purif. Technol.* **2017**, *172*, 388–403. [CrossRef]
7. Wang, S.; Li, P.; Zhang, X.; Zheng, S.; Zhang, Y. Selective adsorption of lithium from high Mg-containing brines using H_xTiO_3 ion sieve. *Hydrometallurgy* **2017**, *174*, 21–28. [CrossRef]
8. Liu, Y.; Zhu, R.; Srinivasakannan, C.; Li, T.; Li, S.; Yin, S.; Zhang, L. Application of Nanofiltration Membrane Based on Metal-Organic Frameworks (MOFs) in the Separation of Magnesium and Lithium from Salt Lakes. *Separations* **2022**, *9*, 344. [CrossRef]
9. Xing, P.; Wang, C.; Chen, Y.; Ma, B. Rubidium extraction from mineral and brine resources: A review. *Hydrometallurgy* **2021**, *203*, 105644. [CrossRef]
10. Page, R.H.; Beach, R.J.; Kanz, V.K.; Krupke, W.F. Multimode-diode-pumped gas (alkali-vapor) laser. *Opt. Lett.* **2006**, *31*, 353–355. [CrossRef] [PubMed]
11. Saliba, M.; Matsui, T.; Domanski, K.; Seo, J.-Y.; Ummadisingu, A.; Zakeeruddin, S.M.; Correa-Baena, J.-P.; Tress, W.R.; Abate, A.; Hagfeldt, A.; et al. Incorporation of rubidium cations into perovskite solar cells improves photovoltaic performance. *Science* **2016**, *354*, 206–209. [CrossRef]
12. Zhang, X.; Tan, X.; Li, C.; Yi, Y.; Liu, W.; Zhang, L. Energy-efficient and simultaneous extraction of lithium, rubidium and cesium from lepidolite concentrate via sulfuric acid baking and water leaching. *Hydrometallurgy* **2019**, *185*, 244–249. [CrossRef]
13. Vieceli, N.; Nogueira, C.A.; Pereira, M.F.; Durão, F.O.; Guimarães, C.; Margarido, F. Recovery of lithium carbonate by acid digestion and hydrometallurgical processing from mechanically activated lepidolite. *Hydrometallurgy* **2018**, *175*, 1–10. [CrossRef]
14. Yan, Q.; Li, X.; Wang, Z.; Wu, X.; Wang, J.; Guo, H.; Hu, Q.; Peng, W. Extraction of lithium from lepidolite by sulfation roasting and water leaching. *Int. J. Miner. Process.* **2012**, *110–111*, 1–5. [CrossRef]
15. Luong, V.T.; Kang, D.J.; An, J.W.; Kim, M.J.; Tran, T. Factors affecting the extraction of lithium from lepidolite. *Hydrometallurgy* **2013**, *134–135*, 54–61. [CrossRef]
16. Sloan, E.D.; Koh, C.A. *Clathrate Hydrates of Natural Gases*, 3rd ed.; CRC Press: Boca Raton, FL, USA, 2008. [CrossRef]
17. Linga, P.; Kumar, R.; Englezos, P. The clathrate hydrate process for post and pre-combustion capture of carbon dioxide. *J. Hazard. Mater.* **2007**, *149*, 625–629. [CrossRef]
18. Ling, Z.; Shi, C.; Li, F.; Fu, Y.; Zhao, J.; Dong, H.; Yang, Y.; Zhou, H.; Wang, S.; Song, Y. Desalination and Li+ enrichment via formation of cyclopentane hydrate. *Sep. Purif. Technol.* **2020**, *231*, 115921. [CrossRef]
19. Truong-Lam, H.S.; Seo, S.D.; Jeon, C.; Lee, G.-P.; Lee, J.D. A gas hydrate process for high-salinity water and wastewater purification. *Desalination* **2022**, *529*, 115651. [CrossRef]
20. Babu, P.; Nambiar, A.; He, T.; Karimi, I.A.; Lee, J.D.; Englezos, P.; Linga, P. A Review of Clathrate Hydrate Based Desalination To Strengthen Energy–Water Nexus. *ACS Sustain.* **2018**, *6*, 8093–8107. [CrossRef]
21. Kumar, A.; Veluswamy, H.P.; Kumar, R.; Linga, P. Direct use of seawater for rapid methane storage via clathrate (sII) hydrates. *Appl. Energy* **2019**, *235*, 21–30. [CrossRef]
22. Veluswamy, H.P.; Linga, P. Natural Gas Hydrate Formation Using Saline/Seawater for Gas Storage Application. *Energy Fuels* **2021**, *35*, 5988–6002. [CrossRef]
23. Gaikwad, N.; Nakka, R.; Khavala, V.; Bhadani, A.; Mamane, H.; Kumar, R. Gas Hydrate-Based Process for Desalination of Heavy Metal Ions from an Aqueous Solution: Kinetics and Rate of Recovery. *ACS EST Water* **2021**, *1*, 134–144. [CrossRef]
24. Tanaka, M.; Tsugane, K.; Suga, D.; Tomura, S.; Ohmura, R.; Yasuda, K. Simultaneous Crystallization of Cyclopentane Hydrate and Sodium Chloride for Desalination and Salt Manufacture. *ACS Sustain.* **2021**, *9*, 9078–9084. [CrossRef]
25. Ito, H.; Gibo, A.; Shiraishi, S.; Yasuda, K.; Ohmura, R. Renewed Measurements of Carbon Dioxide Hydrate Phase Equilibrium. *Int. J. Thermophys.* **2023**, *44*, 128. [CrossRef]
26. Guembaroski, A.Z.; Neto, M.A.M.; Bertoldi, D.; Morales, R.E.M.; Sum, A.K. Phase Behavior of Carbon Dioxide Hydrates: A Comparison of Inhibition Between Sodium Chloride and Ethanol. *J. Chem. Eng. Data* **2017**, *62*, 3445–3451. [CrossRef]
27. Tohidi, B.; Danesh, A.; Todd, A.; Burgass, R. Hydrate-free zone for synthetic and real reservoir fluids in the presence of saline water. *Chem. Eng. Sci.* **1997**, *52*, 3257–3263. [CrossRef]
28. Dholabhai, P.D.; Kalogerakis, N.; Bishnoi, P.R. Equilibrium Conditions for Carbon Dioxide Hydrate Formation in Aqueous Electrolyte Solutions. *J. Chem. Eng. Data* **1993**, *38*, 650–654. [CrossRef]

29. Avlonitis, D.; Danesh, A.; Todd, A. Prediction of VL and VLL equilibria of mixtures containing petroleum reservoir fluids and methanol with a cubic EoS. *Fluid Phase Equilib.* **1994**, *94*, 181–216. [CrossRef]
30. Englezos, P.; Bishnoi, P.R. Prediction of Gas Hydrate Formation Conditions in Aqueous Electrolyte Solutions. *AIChE J.* **1988**, *34*, 1718–1721. [CrossRef]
31. Yasuda, K.; Ohmura, R. Thermophysical Properties of Clathrate Hydrates with Various Guests for Novel Technologies: A Review. *Int. J. Themophys.* **2024**, *45*, 139. [CrossRef]
32. Tohidi, B.; Burgass, R.W.; Danesh, A.; Ostergaard, K.K.; Todd, A.C. Improving the Accuracy of Gas Hydrate Dissociation Point Measurements. *Ann. N. Y. Acad. Sci.* **2000**, *912*, 924–931. [CrossRef]
33. Yasuda, K.; Ohmura, R. Phase Equilibrium for Clathrate Hydrates Formed with Methane, Ethane, Propane, or Carbon Dioxide at Temperatures below the Freezing Point of Water. *J. Chem. Eng. Data* **2008**, *53*, 2182–2188. [CrossRef]
34. Mohammadi, A.H.; Tohidi, B.; Burgass, R.W. Equilibrium Data and Thermodynamic Modeling of Nitrogen, Oxygen, and Air Clathrate Hydrates. *J. Chem. Eng. Data* **2003**, *48*, 612–616. [CrossRef]
35. Maekawa, T. Equilibrium conditions of clathrate hydrates formed from carbon dioxide and aqueous acetone solutions. *Fluid Phase Equilib.* **2011**, *303*, 76–79. [CrossRef]
36. Wang, M.; Sun, Z.-G.; Qiu, X.-H.; Zhu, M.-G.; Li, C.-H.; Zhang, A.-J.; Li, J.; Li, C.-M.; Huang, H.-F. Hydrate Dissociation Equilibrium Conditions for Carbon Dioxide + Tetrahydrofuran. *J. Chem. Eng. Data* **2017**, *62*, 812–815. [CrossRef]
37. Dai, M.L.; Sun, Z.G.; Lim, J.; Huang, H.F. Effect of *n*-dodecane on equilibrium dissociation conditions of carbon dioxide hydrate. *J. Chem. Thermodyn.* **2020**, *148*, 106144. [CrossRef]
38. Mohammadi, A.H.; Anderson, R.; Tohidi, B. Carbon monoxide clathrate hydrates: Equilibrium data and thermodynamic modeling. *AIChE J.* **2005**, *51*, 2825–2833. [CrossRef]
39. Nema, Y.; Ohmura, R.; Senaha, I.; Yasuda, K. Quadruple point determination in carbon dioxide hydrate forming system. *Fluid Phase Equilib.* **2017**, *441*, 49–53. [CrossRef]
40. Kodera, M.; Matsueda, T.; Belosludov, R.V.; Zhdanov, R.K.; Belosludov, V.R.; Takeya, S.; Alavi, S.; Ohmura, R. Physical Properties and Characterization of the Binary Clathrate Hydrate with Methane + 1,1,1,3,3-Pentafluoropropane (HFC-245fa) + Water. *J. Phys. Chem. C* **2020**, *124*, 20736–20745. [CrossRef]

Disclaimer/Publisher's Note: The statements, opinions and data contained in all publications are solely those of the individual author(s) and contributor(s) and not of MDPI and/or the editor(s). MDPI and/or the editor(s) disclaim responsibility for any injury to people or property resulting from any ideas, methods, instructions or products referred to in the content.